Eur Phys J C **40**, s03, 9–13 (2005)
Digital Object Identifier (DOI) 10.1140/epjcd/s2005-03-002-0

EPJ C direct
electronic only

Young Scientist

$\Sigma(1385)$ results with STAR

S. Salur for the STAR Collaboration

Physics Department, Yale University, Sloane Physics Laboratory, P.O. Box 208120, New Haven, CT, 06520-8120, USA,
e-mail: sevil.salur@yale.edu

Received: 21 January 2005 / Accepted: 10 February 2005 /
Published online: 8 March 2005 –

Abstract. This paper introduces the Solenoidal Tracker experiment at the Relativistic Heavy Ion Collider. The corrected p_T spectra and the yields of the $\Sigma(1385)^{\pm}$ and their antiparticles in the most central Au+Au and elementary p+p collisions are presented. Comparison of the $\Sigma(1385)$ $\langle p_T \rangle$ measurement with the other particles corroborates the fact that the $\langle p_T \rangle$ behavior for hyperons (mass> 1.2 GeV) is similar in p+p and Au+Au collisions. The $\Sigma(1385)/\Lambda$ ratio, along with other resonance-to-stable-particle ratios, suggests that a regeneration mechanism recovers the signal loss due to re-scattering in the final state in Au+Au collisions.

PACS. 01.30.Bb

1 Introduction

The Relativistic Heavy Ion Collider (RHIC) [1] is located at Brookhaven National Laboratory (BNL) on Long Island, NY, USA. The circumference of the two independent accelerator rings is 3.8 km. The first collisions took place in the year 2000 and since then collisions of Au+Au at $\sqrt{s_{NN}}$=19, 62, 130, 200 GeV, and p+p and d+Au at $\sqrt{s_{NN}}$=200 GeV have been performed. There are 6 beam interaction points at RHIC and 4 dedicated heavy-ion experiments. BRAHMS [2] and PHOBOS [3] are the two small experiments and the two large ones are PHENIX [4] and STAR [5].

The Solenoidal Tracker At RHIC (STAR) is a large acceptance detector system that is designed to investigate strongly-interacting matter at high energy densities and search for signatures of Quark-Gluon Plasma (QGP), the hadronic deconfinement phase consisting of "free" partons, and its space-time evolution. The physics program of STAR also includes the study of nucleon spin structure functions with polarized p+p collisions, the study of pomeron and photon interactions from intense electromagnetic fields of the colliding ions at RHIC and the study of initial parton distribution functions of the incident nuclei with p+p and d+Au collisions. The p+p and d+Au collisions are also essential for establishing the reference data for heavy ion collisions.

During the expansion of the hot and dense matter (fireball) that is created in heavy ion collisions, chemical freeze-out is reached when the hadrons stop interacting inelastically (see Fig. 1), and elastic interactions continue until thermal freeze-out. Due to the very short lifetime

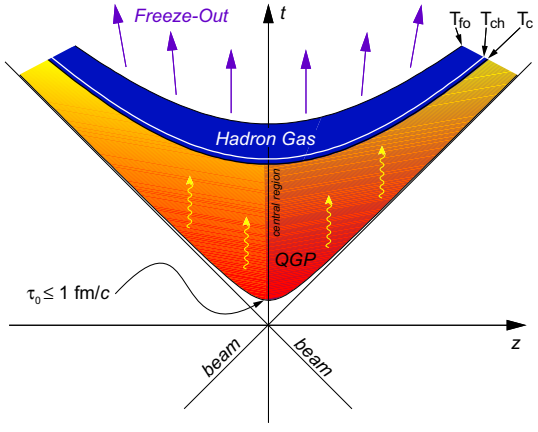

Fig. 1. A lightcone diagram of a collision when QGP is formed. T_{fo} is the abbreviation for thermal freeze-out, while T_{ch} is for chemical freeze-out. The hadronization starts at T_c, the critical temperature

($\tau < \tau_{\rm fireball} \sim$ 10 fm) of most resonances, a large fraction of their decays occur before thermal freeze-out. The decay products interact elastically with the surrounding particles prior to thermal freeze-out, thus resulting in a signal loss for the reconstructed resonances. Secondary interactions (regeneration), however, increase the resonance yield (such as $\Lambda + \pi \rightarrow \Sigma(1385)$). The contribution of re-scattering and regeneration to the total observed yields depends on the time span between the chemical and thermal freeze-out, the lifetime of each resonance, and the regeneration and rescattering probabilities [6,7]. Thus the study of resonances provides an additional tool for deter-

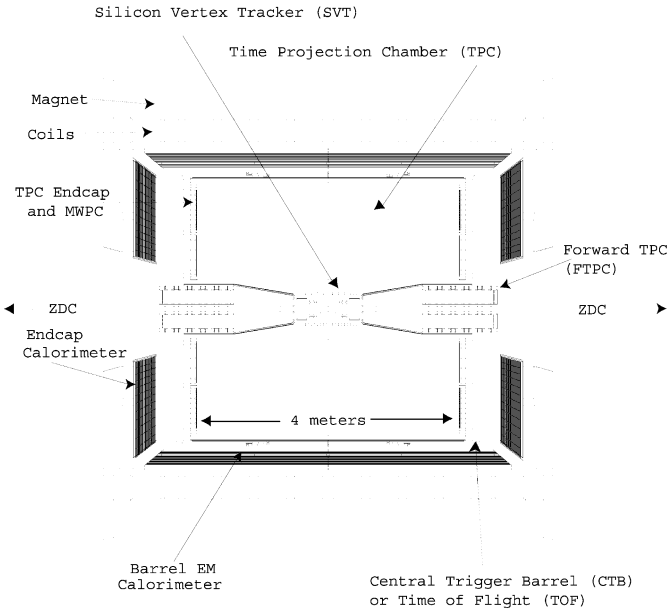

Fig. 2. Side view of the STAR detector configuration. TPC is the main component of the STAR detector used in this analysis

mining the hadronic expansion time between chemical and thermal freeze-out through the comparison of resonance-to-stable-particle ratios.

2 STAR overview and particle identification

A schematic diagram of the components of the STAR experiment is presented in Fig. 2 [5]. The STAR detector's main design features include a Time Projection Chamber (TPC) surrounded by a solenoidal magnet, which has a field of 0.5 Tesla, with an acceptance of $|\eta| < 1.5$ for charged particle tracks [8]. The Silicon Vertex Tracker surrounding the beam pipe improves the resolution of the interaction vertex [9]. In addition, Forward-TPCs increase the rapidity coverage of charged particles to $2.5 < |\eta| < 4$, and electromagnetic calorimeters provide a full azimuthal coverage for high p_T photons, electrons and electromagnetically decaying mesons [10–12]. Glauber model calculations applied to measurements from the zero degree calorimeters (ZDC) in coincidence with the central trigger barrel (CTB) are used to select the most central 5% of Au+Au events. Beam-beam counters and the CTB are used to select minimum bias p+p events.

Charged particles such as π, K, p and e are identified by the energy lost per unit length (dE/dx) and the magnetic field information within the TPC. Figure 3 presents the dE/dx distribution as a function of the momentum of the charged particles in the STAR TPC detector. These charged particles can be clearly identified with the Bethe-Bloch parametrization (solid lines in Fig. 3) up to 800 MeV.

Due to the large acceptance of STAR's detector components, the broad physics program includes precision

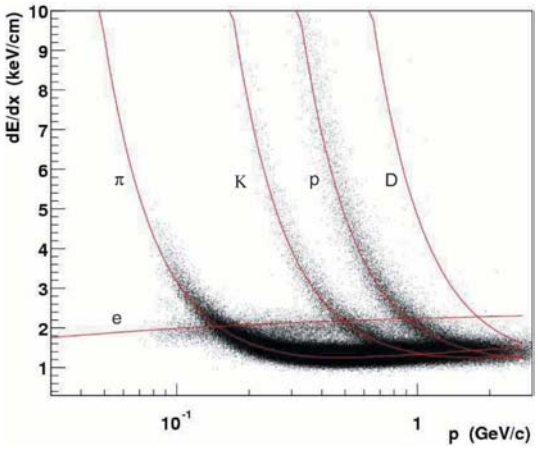

Fig. 3. The energy loss per unit length (de/dx) distribution in the STAR TPC as a function of the momentum of the charged particles

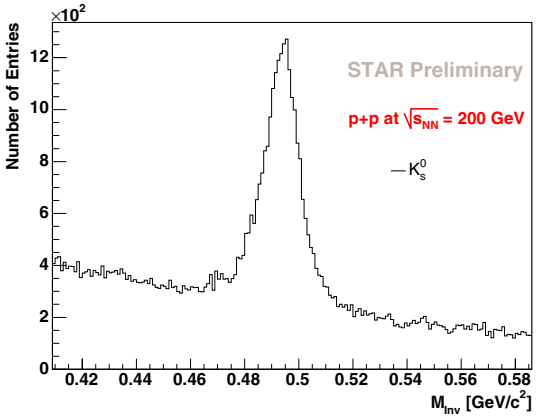

Fig. 4. Invariant mass spectrum for $K^0_s \to \pi^- + \pi^+$ with decay topology information in p+p collisions at $\sqrt{s_{NN}} = 200$ GeV

measurements of a wide variety of strange and charm particles. Long-lived ($c\tau >$ few cm) neutral strange particles, such as Λ and K^0_s, can be reconstructed in the central TPC from their charged decay products. All of the pairs of oppositely charged tracks that originate in the same secondary vertex are selected to represent the decay topology of the neutral particles. Additional geometrical cuts are used to improve the signal-to-background ratio. Signals of K^0_s in Fig. 4, Λ and $\overline{\Lambda}$ in Fig. 5 are presented for p+p collisions at $\sqrt{s_{NN}} = 200$ GeV.

The direct measurement of resonances is not possible due to their short lifetimes (e.g. $c\tau_{\Sigma(1385)} = 5$ fm) [13,14]. The $\Sigma(1385)$ resonances are identified instead through the invariant mass analysis of π and Λ decay particle candidates. A mixed event technique is used to determine the background for uncorrelated pair combinations. The $\Sigma(1385)$ signal is obtained by subtracting this normalized mixed-event background from the invariant mass distribution [15]. The signal before and after the background subtraction is presented in Fig. 6 for p+p collisions at $\sqrt{s_{NN}} = 200$ GeV. Since $\Xi^- \to \Lambda + \pi^-$ shares the same decay channel as $\Sigma^-(1385) \to \Lambda + \pi^-$, we observe both

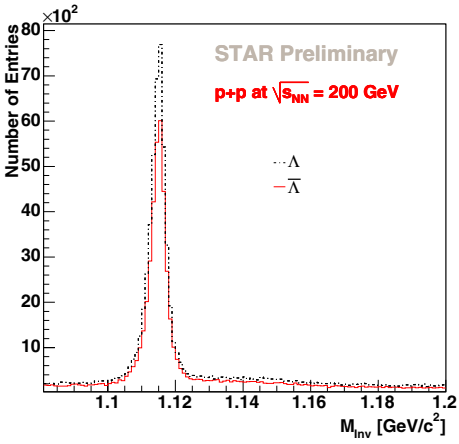

Fig. 5. Invariant mass spectra for $\Lambda \to p+\pi^-$ and $\overline{\Lambda} \to \overline{p}+\pi^+$ with decay topology information in p+p collisions at $\sqrt{s_{NN}} =$ 200 GeV

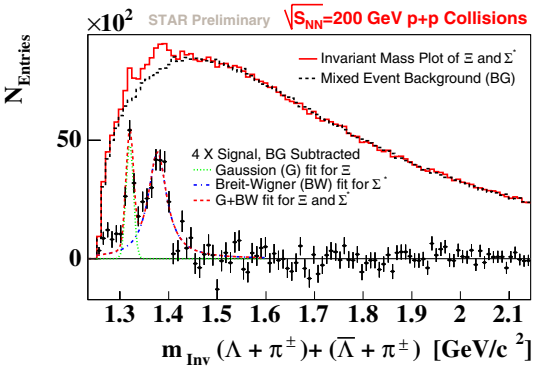

Fig. 6. $\Sigma(1385)$ invariant mass spectra before and after normalized mixed event background subtraction in p+p at $\sqrt{s_{NN}} =$ 200 GeV

signals in the invariant mass spectrum. The background subtracted signal is fitted with a Gaussion for Ξ and a Breit-Wigner for $\Sigma(1385)$.

3 $\Sigma(1385)$ results

The transverse mass (m_T)[1] spectra of $\Sigma^{\pm}(1385)$ and their antiparticles in p+p (open circles) and Au+Au (closed circles) collisions are shown in Fig. 7. The acceptance and efficiency correction for the spectra is accomplished by embedding Monte Carlo simulated resonances into real p+p and Au+Au events. The solid lines in Fig. 7 represent exponential fits to the data with the function directly proportional to the yield (dN/dy) and inversely proportional to the slope parameter $T^2 + m_0 T$ within the framework of a thermal model. The data coverage is 91% and 85% of the fully integrated yield in p+p and Au+Au collisions, respectively. The $\langle p_T \rangle$ is derived from the full range integration of the corresponding exponential fit. For p+p and Au+Au collisions at $\sqrt{s_{NN}} =$ 200 GeV, Table 1 presents inverse slope parameters of the exponential fit functions,

[1] The transverse mass is defined as $m_T = \sqrt{p_T^2 + m^2}$.

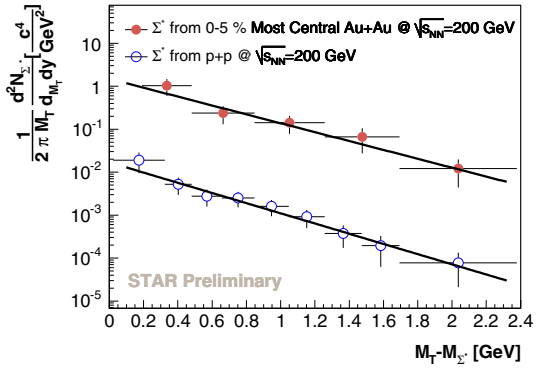

Fig. 7. The transverse mass spectrum for $\Sigma(1385)$ drawn as open circles for p+p and as closed circles for the 5% most central Au+Au collisions at $\sqrt{s_{NN}} =$ 200 GeV. The solid lines represent exponential fits to the data

Table 1. Temperature T, $\langle p_T \rangle$ and yield obtained from the exponential fits of the p_T spectra in Fig. 7 for elementary p+p and 5% most central collisions. The statistical uncertainties are given and the systematic error, mostly due to normalization and the shape of the background, $\sim$ 15%, must be included in the given values

$\Sigma^{\pm}(1385)$	p+p	Au+Au
T [MeV]	358 ± 47	420 ± 84
$\langle p_T \rangle$ [MeV]	1.08 ± 0.15	1.20 ± 0.24
Yields (dN/dy)	$(4.66 \pm 0.98)10^{-3}$	4.72 ± 1.38

the $\langle p_T \rangle$s and the yields (dN/dy) of the summed signal of $\Sigma^{\pm}(1385)$ and their antiparticles.

The $\langle p_T \rangle$ as a function of particle mass for p+p and Au+Au collisions at $\sqrt{s_{NN}} =$ 200 GeV is presented in Fig. 8. The behavior of $\langle p_T \rangle$ vs. mass for the various particles in p+p and Au+Au collisions is compared to two parameterizations. The triangles represent the short-lived resonances and the circles indicate long-lived stable particles. The black curve is an empirical fit to the ISR π, K and p data in p+p collisions and the band is a blast wave fit using π, K and p in STAR Au+Au collisions [16, 17]. The empirical parametrization for the ISR data at $\sqrt{s} =$ 25 GeV in p+p collisions can describe the behavior of the lower mass particles, such as π, K and p, despite the fact that our collision energy is one order of magnitude higher. However, this empirical parametrization does not represent the behavior of the higher mass particles in p+p collisions. Similarly, the blast wave parametrization, which can describe the lower mass particles ($\sim$ 98% of all the particles observed) in Au+Au collisions, fails to explain the behavior of higher mass particles.

The heavy particles in p+p and Au+Au collision show a similar behavior of $\langle p_T \rangle$. It is expected that resonances with higher transverse momentum are more likely to be reconstructed because they have longer relative lifetimes due to Lorentz contraction, which means that they are more likely to decay outside of the medium. As a consequence, their daughter particles should interact less with the medium in Au+Au collisions. Any loss at low p_T would

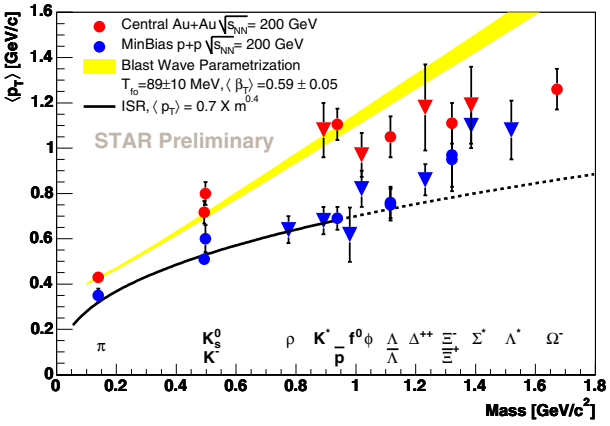

Fig. 8. The $\langle p_T \rangle$ vs particle mass measured in p+p and Au+Au collisions at $\sqrt{s_{NN}}$ = 200 GeV. The black curve represents the ISR parametrization from π, K and p for $\sqrt{s_{NN}}$ = 25 GeV p+p collisions. The yellow band is the blast wave fit using π, K and p for Au+Au collisions

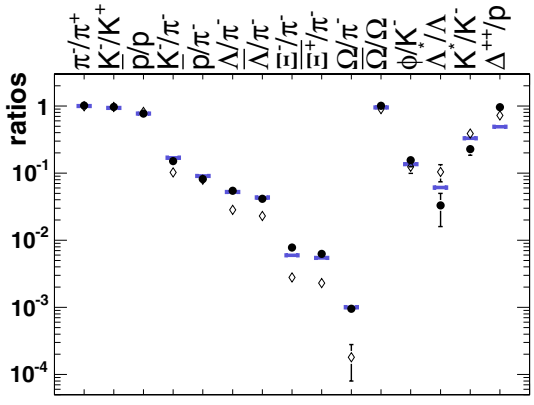

Fig. 9. Particle ratios in $\sqrt{s_{NN}}$ = 200 GeV p+p (open diamonds) and Au+Au (solid circles) collisions as compared to thermal model (solid lines) predictions with T_{ch} = 160 MeV, μ_B = 2.65, μ_s = 1.31, γ_s = 0.99 [25]

increase the T parameter of the p_T spectra for the central Au+Au collisions with respect to p+p collisions. However we do not see any significant increase in the T parameter for $\Sigma(1385)$ from p+p to the most central Au+Au collisions within the statistical and systematic errors. This might be due to our p+p reference data. The higher mass particles might be produced in more violent (mini-jet) p+p collisions than the lower mass particles, so that the $\langle p_T \rangle$ for heavy particles in p+p collisions would be higher. In Au+Au collisions there is evidence that heavier particles flow radially at a lower velocity than the lighter mass particles (such as π mesons). These two independent effects in p+p and Au+Au collisions might cause the apparent merging of the $\langle p_T \rangle$ which is corroborated by the $\Sigma(1385)$ measurement.

The resonance production also presents an important test of thermal production and hydrodynamics models. The ratio of resonances to their stable particles are insensitive to fugacities and phase space occupancies [24]. Figure 9 presents a comparison between the thermal model

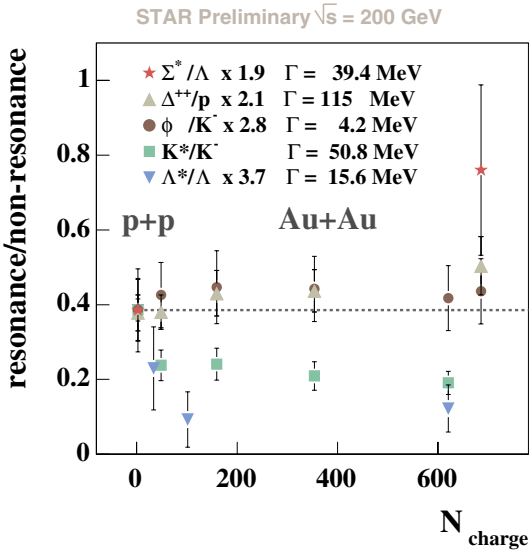

Fig. 10. Resonance to stable particle ratios of ϕ/K^- [19], Δ^{++}/p [20], $K^*(892)/K^-$ [21], $\Sigma(1385)/\Lambda$ and $\Lambda(1520)/\Lambda$ [22, 23] for p+p and Au+Au collisions at $\sqrt{s_{NN}}$ = 200 GeV. The ratios are normalized to the ratio of $K^*(892)/K^-$ in p+p collisions. Statistical and systematic errors are included

predictions and the measured particle ratios [25]. Lines represent the thermal model predictions, the open diamonds indicate p+p collisions and closed circles are for Au+Au collisions. The thermal model accurately describes the stable particle ratios in both p+p and Au+Au collisions. However, the deviations observed for the resonance particles are large and must be investigated. Regeneration and rescattering are excluded in thermal models, which might suggest one explanation for why the experimental values differ from the calculations of the statistical model for most of the resonances.

The measurements of the ratios of resonances to stable particles as a function of charged particle multiplicity for $\Sigma(1385)$ and other resonances are presented in Fig. 10. The observed suppression of $\Lambda(1520)/\Lambda$ and $K^*(892)/K$ from peripheral to most central Au+Au collisions compared to p+p collisions is in agreement with a rescattering scenario of the decay particles in the dense medium that causes a signal loss. The $\Sigma(1385)/\Lambda$ ratio does not show this suppression (within errors) for the 5% most central Au+Au collisions in comparison to the p+p collision environment, even though $c\tau_{\Sigma(1385)} < c\tau_{\Lambda(1520)}$, which should cause more rescattering for $\Sigma(1385)$. Therefore a strong regeneration cross section has to be assumed for the $\Lambda + \pi \rightarrow \Sigma(1385)$ in order to recover the signal loss due to rescattering. Resonance-to-stable-particle ratios can also be used to test microscopic (UrQMD) models, which include rescattering and regeneration in their calculations. The UrQMD model prediction in Fig. 11 shows the collision energy dependence of the $\Sigma^{\pm}(1385)/\Lambda$ ratios for Au+Au collisions. The measured $\Sigma^{\pm}(1385)/\Lambda$ ratio is 0.295 ± 0.086 for the 5% most central Au+Au collisions, which is about a factor of 2 below the UrQMD prediction at $\sqrt{s_{NN}}$ = 200 GeV. The regeneration cross section as-

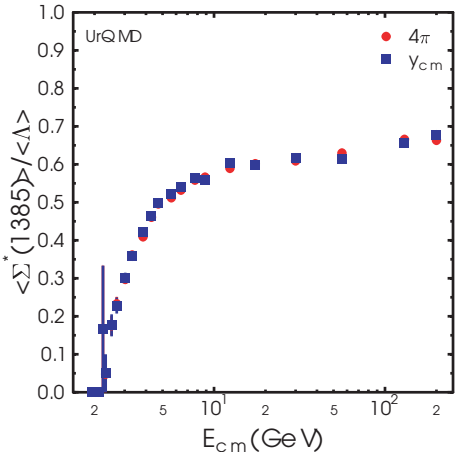

Fig. 11. Collision energy dependence of $\Sigma^{\pm}(1385)/\Lambda$ ratios for Au+Au collisions predicted by the microscopic models (UrQMD). Plot from M. Bleicher [18]

sumed in UrQMD appears to be too high and has to be revised in light of these resonance measurements.

4 Conclusions

$\Sigma^{\pm}(1385)$ resonances and their anti-particles can be reconstructed via event mixing techniques in p+p and Au+Au collisions with the STAR detector. The $\Sigma(1385)$ $\langle p_T \rangle$ in p+p collisions is similar (within the errors) to that measured in Au+Au collisions. This follows the behavior of the other high mass particles ($m > 1.2$ GeV) whose $\langle p_T \rangle$ measurement in p+p approaches the Au+Au value. This behavior suggests a smaller radial flow for heavy particles and/or the preferred production of heavy particles from hard scattering and jet fragmentation in p+p collisions.

No significant suppression is observed in the $\Sigma(1385)/\Lambda$ ratios from p+p to the 5% most central Au+Au collisions. Since the previously measured suppression of K*(892)/K and $\Lambda(1520)/\Lambda$ ratios agrees with a signal loss due to rescattering in the medium, the null suppression of the $\Sigma(1385)$ ratio suggests a significant regeneration mechanism for recovering the signal lost via rescattering [18,24]. Current statistical and microscopic models need to be modified to account for the resonance measurements coming from heavy ion collisions.

The event mixing technique clearly works well for resonance identification. The same technique is being used in the search for the Θ^+ pentaquark, a five-quark bound system consisting of uudd$\bar{s}$ and other exotic particles [26].

References

1. M. Harrison et al., Nucl. Inst. Meth. A **499**, 235 (2003)
2. K.H. Adamczyk et al., Nucl. Inst. Meth. A **499**, 437 (2003)
3. B.B. Back et al., Nucl. Inst. Meth. A **499**, 603 (2003).
4. K. Adcox et al., Nucl. Inst. Meth. A **499**, 469 (2003)
5. K.H. Ackermann et al., Nucl. Inst. Meth. A **499**, 624 (2003)
6. G. Torrieri, J. Rafelski, Phys. Lett. B **509**, 239 (2001)
7. M. Bleicher, J. Aichelin, Phys. Lett. B **530**, 81 (2002)
8. M. Anderson et al., Nucl. Inst. Meth. A **499**, 659 (2003)
9. R. Bellwied et al., Nucl. Inst. Meth. A **499**, 640 (2003)
10. K.H. Ackermann et al., Nucl. Inst. Meth. A **499**, 713 (2003)
11. M. Beddo et al., Nucl. Inst. Meth. A **499**, 725 (2003)
12. C.E. Allgower et al., Nucl. Inst. Meth. A **499**, 740 (2003)
13. C. Adler et al., STAR Collaboration, Phys. Rev. C **65**, 041901 (2002)
14. C. Adler et al., STAR Collaboration, Phys. Rev. C **66**, 061901 (2002)
15. S. Salur, for the STAR Collaboration, NATO Science Series II, **166**, 665 (2004) hep-ex/0403016
16. M. Bourquin, J.-M. Gaillard, Nucl. Phys. **114**, 334 (1976)
17. J. Adams, STAR Collaboration, Phys. Rev. Lett. **92**, 182301 (2004)
18. Marcus Bleicher, Nucl. Phys. A, **715**, 85 (2003)
19. J. Ma, for the STAR Collaboration, J. Phys. G **30**, S543 (2004)
20. Z. Xu, J. Phys. G **30**, S325 (2004)
21. H. Zhang, for the STAR Collaboration, J. Phys. G **30**, S577 (2004)
22. L. Gaudichet, for the STAR Collaboration, J. Phys. G **30**, S549 (2004)
23. Ch. Markert, for the STAR Collaboration, 19th Winter Workshop on Nuclear Dynamics 71 (2003)
24. G. Torrieri, J. Rafelski, Phys. Rev. C **68**, 061901 (2003)
25. O. Barannikova, for the STAR Collaboration, Private Communication
26. S. Salur, for the STAR Collaboration, nucl-ex/0403009